Author(s): Sullivan, Angus I.; DeJesus, Joseph F.; Malola, Sami; Takano, Shinjiro; Tsukuda, Tatsuya; Häkkinen, Hannu; Crudden, Cathleen M.

Title: Synthesis and Characterization of a Monodentate N-Heterocyclic Carbene-Protected Au11-Nanocluster via Reduction with KC8

Year: 2023

Version: Accepted version (Final draft)

Please cite the original version:

Sullivan, A. I., DeJesus, J. F., Malola, S., Takano, S., Tsukuda, T., Häkkinen, H., & Crudden, C. M. (2023). Synthesis and Characterization of a Monodentate N-Heterocyclic Carbene-Protected Au11-Nanocluster via Reduction with KC8. Chemistry of Materials, 35(7), 2790-2796. https://doi.org/10.1021/acs.chemmater.2c03429

Synthesis and Characterization of a monodentate *N*-Heterocyclic Carbene-Protected Au_{11}-Nanocluster *via* Reduction with KC_8

Angus I. Sullivan,[a] Joseph F. DeJesus,[a]† Sami Malola,[b] Shinjiro Takano,[c] Tatsuya Tsukuda*,[c] Hannu Häkkinen*,[b] and Cathleen M. Crudden*[a][d]

[a] Department of Chemistry, Queen's University, Chernoff Hall, Kingston, Ontario K7L 3N6, Canada.

[b] Department of Chemistry and Physics, Nanoscience Center, University of Jyväskulä, 40014, Jyväskulä, Finland.

[c] Department of Chemistry, Graduate School of Science, The University of Tokyo, 7-3-1 Hongo, Bunkyo-ku, Tokyo, 113-0033, Japan.

[d] Institute of Transformative Bio-Molecules (WPI-ITbM), Nagoya University, Chikusa, Nagoya 464-8602, Japan

ABSTRACT: Atomically precise gold nanoclusters are an exciting and growing class of nanomaterial. While normally protected with ligands such as thiols or phosphines, gold nanoclusters protected with N-heterocyclic carbenes (NHCs) have recently garnered attention due to potential improvements in stability and optical properties of the resulting clusters. However, as this field is in its infancy, little work has been done with reducing agents beyond sodium borohydride ($NaBH_4$), a reagent that dominated synthetic efforts in other clusters as well. Herein, we report the use of potassium intercalated graphite (KC_8) in the synthesis of nanoclusters, and the novel Au_{11}-nanocluster protected with monodentate NHC ligands it produces, $[Au_{11}(NHC)_8Br_2]Br$. The cluster is characterized by ESI-MS, UV-Vis spectroscopy, ^1H and $^{13}C\{^1H\}$ NMR. Starting from a partially resolved X-ray crystal structure showing the heavy atoms, DFT calculations enable us to propose a total structure.

1. INTRODUCTION

Gold nanoclusters are a class of nanomaterials which have promise in a variety of applications including imaging, cancer chemotherapy and catalysis.[1] Nanoclusters offer the advantage over nanoparticles in that monodisperse clusters of specific chemical formula and distinct properties can be reproducibly synthesized in solution and characterized using crystallography and spectroscopy.[2] N-Heterocyclic carbene (NHC) ligands are attracting interest as surface ligands for nanoclusters because their properties appear to mimic phosphines in terms of ligation behavior and thiols in terms of cluster stability.[3, 4]

The first mixed valence Au(0)/Au(I) clusters stabilized fully by NHC ligands were Au_3 clusters reported by Sadighi and subsequently Bertrand.[5, 6] In 2019, our group reported the first use of NHCs to protect Au_{11}[4] and Au_{13}[3] nanoclusters. Since then, our group along with Han, Zang, Tsukuda, Mak, and Zheng have reported the synthesis of Au_{10}[7], Au_{11}[8], Au_{13}[8-10], Au_{23}[11], Au_{24}[12, 13], Au_{25}[13-15], and Au_{44}[16] nanoclusters protected by NHCs.

Synthetic routes to these NHC-stabilized Au nanoclusters have employed one method only: the reduction of Au(I)-NHC complexes by sodium borohydride. Since the reducing agent has a large effect on the size and size distribution of nanocluster products, examining alternative reducing agents is a critical next step in advancing this work.[17] In traditional thiolate-stabilized clusters, milder reducing agents such as carbon monoxide and amine boranes have been employed, but remarkably, there have been few methods published employing alternative reducing agents in this domain either.[16, 18-25]

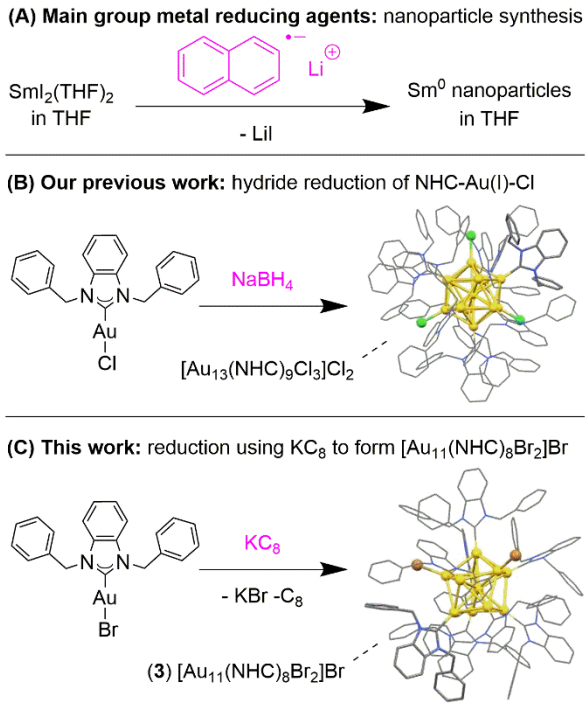

Scheme 1. (A) Use of dissolving metal reducing agent to form unligated nanoparticles[26], (B) our group's previous work with NHC protected gold nanoclusters[3] and (C) this work.

Before the widespread use of $NaBH_4$, the organometallic reagent $Ti(\eta\text{-}C_6H_5CH_3)_2$ was employed as a reducing agent in the synthesis of phosphine protected Au_9, Au_{11}, and Au_{13} nanoclusters.[27-29] More recent examples include the use of dissolving metal reductants where the metal is actually incorporated in the cluster. For example Schnepf et al. synthesized the gallium doped nanocluster $[Au_9Ga(PPh_3)_8Cl_2]^{2+}$ using GaCp (Cp = cyclopentadienyl) as the reducing agent and gallium source.[30] In a rare example of a clean one electron reducing agent that is not incorporated in the cluster, a novel Ag_{18} nanocluster was prepared using radicals generated in a Norrish type I photochemical cleavage as the reducing agent by Stamplecoskie et al.[31]

Herein we describe the first example of the use of KC_8 as a reducing agent for the synthesis of ligand-protected nanoclusters (Scheme 1). Precision one electron reducing agents such as Na and Li naphthalenide are common in organic and inorganic chemistry for the quantitative transfer a single electrons and halide removal,[32, 33] but they are virtually unexplored in materials synthesis. To date, these reagents have only been reported use for the preparation of nanoparticles of unligated metal nanoparticles such as Sm(0) and Fe(0) (Scheme 1).[26, 32]

2. RESULTS AND DISCUSSION

We began our study by using KC_8 as the reducing agent and NHC-Au-Br as the NHC/Au source. This resulted in the production of a new monodentate NHC-ligated $[Au_{11}(NHC)_8Br_2]Br$ cluster. While phosphine protected $[Au_{11}(PPh_3)_8Cl_2]Cl$ and $Au_{11}(PPh_3)_7Cl_3$ clusters are known[35], as of yet, there are no examples of the corresponding Au_{11} cluster fully protected by NHCs. The synthesis of an NHC analogue to these important phosphine-protected clusters represents a valuable comparison tool to learn more about their stability and reactivity.[34,35]

NHC gold(I) complex (**2a**) was synthesized following literature procedures (see SI).[36] The low temperature reduction (0 °C) of **2a** in THF using 2 equivalents of KC_8 in the presence of 0.7 equivalents of dibenzo-18-crown-6 causes the colorless solution to turn vibrant red. The strong color changes led us to examine the reaction by UV-Vis spectroscopy, monitoring the increase in the absorbance band at 416 nm as representative of the gold nanocluster compared to a loss of the UV absorbance peak at 290 nm attributable to the gold complex **2a**. After the reaction was deemed complete, it was quenched by filtration through Celite® to remove excess KC_8. Through ^1H NMR analysis of crude reaction mixtures after reduction, it was found that **2a** was mostly consumed when the band at 416 nm was 10 % of the intensity of the peak at 290 nm (Figure S5 & S32), which corresponded to 2 – 6 h depending on stirring speed. It was important to accurately determine the endpoint of the reaction because allowing the reduction to continue past this point causes visible decomposition of the gold nanocluster represented by a color change of the solution from red to brown.

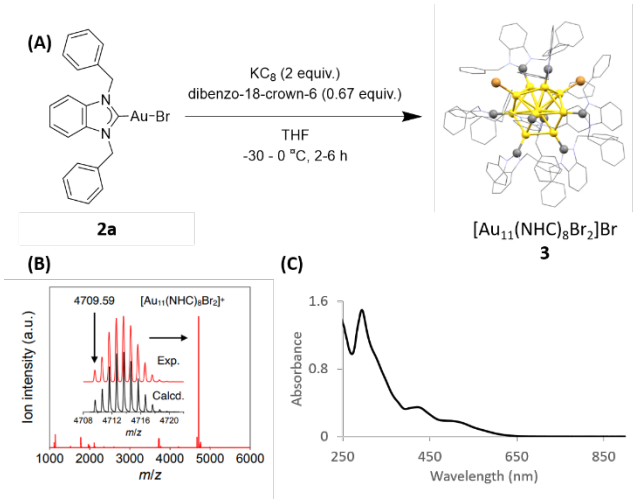

Figure 1. Synthesis and characterization of $[Au_{11}(NHC)_8Br_2]Br$ via reduction of **2a** (A) General reaction conditions for the synthesis (B) ESI-MS of the Au_{11} cluster (C) UV-Vis spectrum of the nanocluster in THF.

ESI-MS analysis resulted in a set of signals at m/z 4709.59 which were assigned to the novel gold nanocluster $[Au_{11}(NHC)_8Br_2]Br$ (**3**) (Figure 1). Purification of the cluster was achieved by removing more soluble species like **2a**, [NHC-Au-NHC]Br, and crown ether in 2:1 pentane:THF washes at room temperature. The process was repeated until these impurities were removed, as evidenced by the loss of a shoulder peak at 280 nm in the UV-Vis spectrum (see Figure S5 and S32). Under these work-up conditions, the cluster can be obtained in 62% yield at ca. 80 % purity based on ^1H NMR integration of the methylene protons of **3**. Further purification of **3** can be accomplished by exhaustive extraction into toluene and mixtures of pentane and THF (pentane:THF 1:9), but due to the low increase in sample purity after these extractions, further manipulations of **3** were conducted with the 80% pure material (Figure S29). Attempts to optimize the reaction further, by decreasing concentrations and temperatures, resulted in slower reactions with no improvement in selectivity or yields. Longer reaction times and higher temperatures (22 °C) resulted in lower selectivity for the Au_{11} nanocluster giving rise to the formation of disperse and intractable cluster mixtures (Figure S33).

From these samples, pure crystals can be grown in low yields by layering -40 °C pentane over a dilute solution of **3** in -40 °C THF (pentane:THF 4:5). Impurities can be removed from the crystals by washing with cold THF (-40 °C). These crystals were characterized by ESI-MS, UV-Vis spectroscopy and NMR spectroscopy.

ESI-MS of crystalline **3** revealed that the only high molecular weight molecular species present was consistent with the mass of $[Au_{11}(NHC)_8Br_2]^+$. Further characterization by UV-Vis spectroscopy of the crystalline sample, which is red in both the solid state and in solution, demonstrated characteristic absorption bands at 425 nm and at 520 nm. This is similar to the absorption bands seen for the previously reported $[Au_{11}(PPh_3)_8Cl_2]Cl$ cluster which has an absorbance band at 416 nm and a broad band at 500 nm.[35] The phosphine-protected cluster also demonstrated a small absorbance band at 312 nm, which is not clearly seen for **3**.

The purified cluster demonstrates only one ligand environment in ^{1}H NMR and $^{13}C\{^{1}H\}$ spectra (Figures 3, S24 and S25). The nanocluster has a single carbene carbon signal at 211 ppm which is clearly visible without carbon isotope labelling of the carbenic carbon (Figure 2). This highly deshielded carbene signal is consistent with all other reported NHC-protected gold nanoclusters.[3,7,12] A single resonance peak for the carbene in $^{13}C\{^{1}H\}$ NMR is consistent with the single phosphine chemical shift seen in ^{31}P NMR for the $[Au_{11}(PPh_3)_8Cl_2]Cl$ cluster, and suggests that exchange processes are taking place in solution on the NMR time scale.[35] The NHC-containing cluster $[Au_{11}(PPh_3)_7(NHC)Cl_2]Cl$ demonstrated similar behaviour.[4] Variable low temperature (VT) ^{1}H NMR experiments with the cluster **3** resulted in decoalescence of the benzyl-methylene peak supporting the presence of an exchange process for this cluster (Figure 2D).

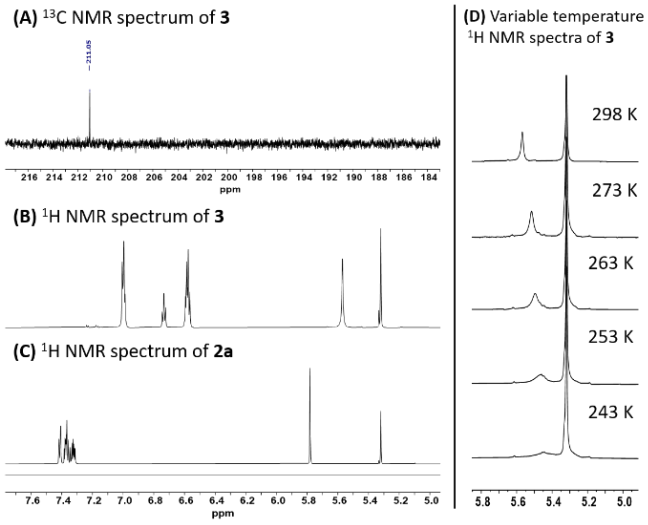

Figure 2. (A) $^{13}C\{^{1}H\}$ NMR carbene chemical shift of $[Au_{11}(NHC)_8Br_2]Br$ (B) ^{1}H NMR spectrum of $[Au_{11}(NHC)_8Br_2]Br$ crystals (C) ^{1}H NMR spectrum of Br-Au-NHC (D) variable temperature analysis of the benzylic Au_{11} -CH_2- resonance peak in ^{1}H NMR.

Attempts to gain a full understanding of solid-state structure by single crystal X-ray crystallography were hampered by difficulties obtaining high quality crystals. These include inherent difficulties in crystalizing gold nanoclusters[37,38], the lack of stability of **3** in various solvents, and decomposition during attempted anion exchange experiments (see Figure S7-13, S34). Solution stability studies (Figure S7-13) confirmed that while cluster **3** showed no sign of decomposition in typical organic solvents at room temperature, decomposition was observed upon heating or in the presence of water.

The thermal stability of **3** was directly compared to $[Au_{11}(PPh_3)_8Cl_2]Cl$ by heating both clusters in acetonitrile and toluene, and monitoring decomposition by UV-Vis spectroscopy.[3,4,39] Thermal treatment of both clusters in acetonitrile at 70 °C resulted in decomposition in a similar timeframe indicating comparable stability (Figure S35).[3] The decomposition of **3** could not be monitored effectively at 70 °C in toluene due to the conversion of **3** to other species with overlapping absorbance bands including $[Au_{13}(NHC)_9Br_3]Br_2$ (Figures S36-38).

However, lower quality crystals could be generated by layering hexanes over a solution of **3** in THF (both solvents at a temperature of -40 °C). From these crystals, X-ray crystallography confirmed the expected $Au_{11}Br_2$ core. Reliable confirmation of exact placement of the atoms in the organic shell was not possible. Considering these limitations, we turned to density-functional theory (DFT) studies to provide insight into the full structure.

DFT and time-dependent density functional theory (TDDFT) calculations were performed to study the structure as well as the electronic and optical properties of the synthesized cluster $[Au_{11}(NHC)_8Br_2]^{+}$. The calculations were performed using the software GPAW[40] with two different xc-functionals; Perdew-Burke-Ernzerhof (PBE)[41] and BEEF-vdW[42]. The initial structure was built based on the partially resolved experimental structure, from which only positions of the metal atoms and halides could be reliably determined. It was relatively straightforward to complete the structure of the metal-ligand interface with 8 carbenes in top positions as there are in total 10 surface Au-atom sites in the Au-core and two bromide atoms were already resolved (See SI).

The stability and dynamics of the generated structure model was confirmed by a molecular dynamics (MD) simulation with DFT forces that included heating to ~300 K, a production run, and annealing the system back to low temperatures below 50 K. The MD run was done to confirm the thermal stability of the model structure and the dependence of the results on the exact ligand layer conformation. The MD results are discussed later on. All the calculated structures were optimized before the detailed analysis.

The electronic structure of the optimized initial model structure was analyzed by projecting the density of electronic states to spherical harmonics (Ylm) functions centered at the center of mass of the cluster. The analysis can be used to characterize the superatom states of the cluster which are delocalized on the metal core.[42] As expected by the composition of the cluster, 11 free valence s-electrons in Au-atoms, 2 electron withdrawing bromides, and the 1+ total charge result in an 8e superatom system. This is confirmed by the Ylm-analysis shown in Figure 3a (PBE functional) that clearly shows three P-symmetric states as the highest occupied states and D-symmetric states as the lowest unoccupied states. The BEEF-vdW functional gives almost identical results with only moderate changes in positions and degeneracy of the states as shown in Figure S39A.

Differences between the nature of the ligands is seen in the Bader charges of atoms listed in Table S2. Bromides are negatively charged -0.516 |e| whereas carbenes are positively charged by +0.315 |e|. Metal atoms in the surface of the core are nearly neutral -0.018 |e| regardless of the capping ligand group bound to them while the central Au-atom is negatively charged by -0.311 |e|.

The electronic structure directly affects the optical response. The calculated optical absorption spectrum of the optimized model structure is shown in Figure 3B. The overall agreement to experimental spectrum is reasonably good. There are three identifiable low energy features in the calculated spectrum, the lowest one in energy being much broader than the two other. The second lowest peak is located below 450 nm both experimentally and computationally. Below 350 nm there is a steep enhancement in the absorption intensity followed by distinguished high energy absorption peaks close to 300 nm. Compared to experiments, the optical gap is underestimated,

the edge of the absorption tail being at 650 nm (1.9 eV) experimentally and 750 nm (1.7 eV) computationally.

The HOMO-LUMO energy gap of the system matches with the optical gap, which is determined by the dipole allowed transitions between P to D states based on the general selection rules. The underestimation of the HOMO-LUMO gap with PBE functional is expected because of the tendency to expand the metal core structure compared to true realistic size. Some minor discrepancy is also seen in the shape of the high energy features that are merged into one main peak in experimental spectrum. The measured spectrum still clearly shows a non-symmetric shape with faint side features on both sides of the maximum. These may coincide with the more pronounced features seen in the calculated spectrum. The spectrum calculated with BEEF-vdW (see Figure S39B) is almost identical to the PBE spectrum. Because of the consistency in the results we decided to concentrate on the PBE functional with molecular dynamics (MD) simulations that are described next.

MD simulations were carried out to confirm the stability of the model cluster and to examine the effects of the exact ligand-layer conformation to the absorption spectrum. The MD simulations were run using Langevin thermostat in total for 11.7 ps using the PBE functional. The MD simulation included heating using target temperature of 300 K, a production run at ~300 K and annealing the system back to low temperatures. The simulation was stopped when the temperature was dropped below 50K.

The structure stayed intact during the whole MD-run and only the organic part of the ligand layer becomes reoriented. No drastic changes were seen in the overall structure. The optimized initial model structure and the final MD-step structures are visualized in Figure S40A and S40B respectively. After annealing the structure back to low temperatures, the electronic structure and optical absorption spectrum were calculated for the optimized snapshot structure of the final step for which results are shown in Figure S41. The electronic structure (Figure S41A) is comparable to the electronic structure before the MD-run (Figure 3). The HOMO-LUMO gap and the positions of the states follow closely the results of the initial model structure. As a consequence, changes in the absorption spectrum are also minimal. The lowest energy peak becomes slightly sharper and the other peaks smoothen. This may relate to redistribution of the ligand states. Otherwise the spectrum remained unchanged and assignment of the features with respect to the measured spectrum remained the same.

To conclude, we showed that the model structure is stable, reproduces the experimental results and can explain the detailed structure of the measured cluster.

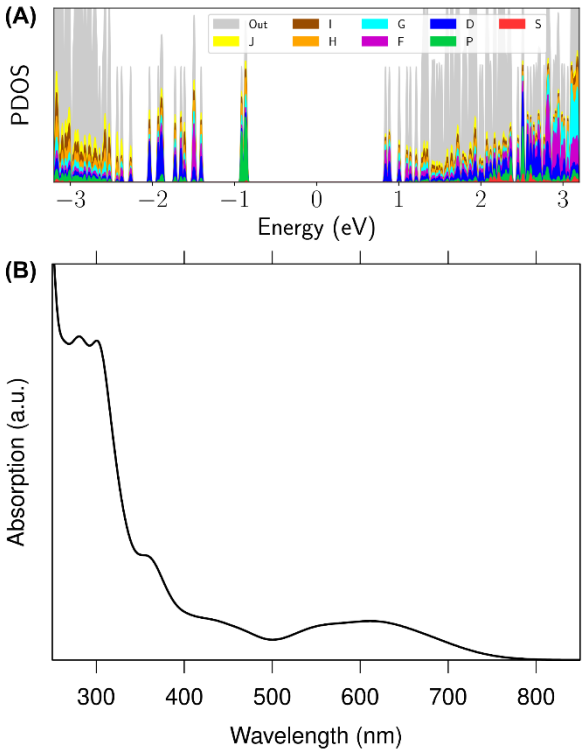

Figure 3. Calculated results with PBE functional for A) projected density of states of optimized model cluster $[Au_{11}(NHC)_8Br_2]^+$ mapping the symmetries of superatom states based on spherical harmonics functions centered at the center of the mass of the cluster and (B) optical absorption spectrum of the same structure. Different colors denote different angular momenta.

To test the effect of the halide on the nature of the product formed, we also reduced NHC-Au-Cl with KC_8. As with the bromide starting material, reduction with KC_8 took place, giving $[Au_{11}(NHC)_8Cl_2]Cl$ as the major product (Figure S43-46). The cluster peak is seen in ESI-MS and is identified in the NMR spectra based on the carbene chemical shift of 211 ppm. However, nanocluster formation occurred at a slower rate with the chloride compared to the reduction of bromide **2a** (Figure S43). More side products were also observed with the chloride (Figure S44-46).

Similarly, reduction of bromide salt **2a** with $NaBH_4$ in EtOH/DCM, conditions which previously produced Au_{13} clusters,[3] gave $[Au_{13}(NHC)_9Br_3]Br_2$ as the major cluster product, not Au_{11} (Figure S47). The reduction of **2a** with $NaBH_4$ in THF under inert atmosphere does not result in the formation of any nanoclusters (Figure S48). These experiments demonstrate that the observed Au_{11} nanocluster is formed because of the nature of the reducing agent (KC_8 vs. $NaBH_4$) rather than the halide.

To examine the generality of the synthetic method, related gold complexes **2b** and **2c** were treated with KC_8 at -40 °C (Scheme 2). Reduction of **2b** resulted in a polydisperse mixture of Au_9, Au_{10}, and Au_{11} nanoclusters with Au_{11} being the minor product as seen in ESI-MS (Figure S1 and S2). Compound **2c** gave fast decomposition to a brown solution with no evidence of cluster formation at the point of analysis (Figure S3).

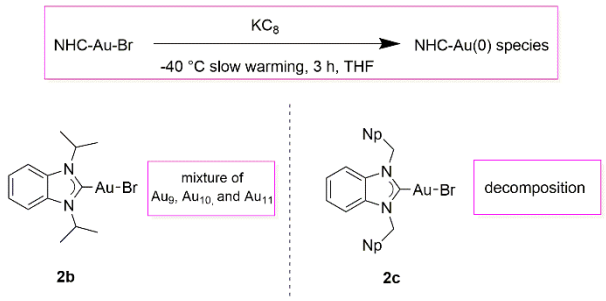

Scheme 2. General conditions for the reduction of **2b** and **2c**, and the results thereof.

While it is perhaps not surprising that replacing the N-benzyl substituent in **2a** with isopropyl substituents as in **2b** was unsuccessful (although we note the successful use of this ligand in cluster synthesis by the Zheng group)[9, 14, 16] the failure of the naphthyl-substituted cluster was more surprising. One possibility we considered is that the π-extended aromatics served as a second point of reaction with KC_8, since species like LiNp are well known. Instability of any initially generated clusters in the presence of the strong reducing agent is another possibility. Regardless, these results suggest that while KC_8 is clearly an effective reducing agent for the preparation of nanoclusters from molecular Au NHC species, optimization of individual reactions is likely necessary, taking into consideration the stability of the starting materials and the final nanoclusters.

3. CONCLUSIONS

In conclusion, we have demonstrated that a main group metal reducing agent, specifically KC_8, can be employed for the generation of Au nanoclusters stabilized by N-heterocyclic carbenes. Using the same molecular NHC–Au precursor, clusters with different cores were obtained. Specifically, the KC_8 method gave clusters with the formula $[Au_{11}(NHC)_8Br_2]Br$, reminiscent of Hutchinson's Au_{11} phosphine clusters[35], while reduction of this same precursor with $NaBH_4$ gives $[Au_{13}(NHC)_9Cl_3]Cl_2$.[3] Unlike these NHC-stabilized Au_{13} clusters, the Au_{11} clusters produced herein have higher reactivity, a property our group will be exploring in catalytic applications of these clusters. The study of alternative single electron reducing agents for the synthesis of metal clusters inaccessible by reduction with $NaBH_4$ is ongoing in our lab.

4. EXPERIMENTAL METHODS

4.1 Materials and Methods

All NHC ligands and Au(I) NHC complexes were synthesized under ambient conditions. Reductions using KC_8 and manipulations of $[Au_{11}(NHC)_8Br_2]Br$ were done under inert atmosphere in a N_2 filled glovebox. Unless otherwise stated, all reagents were purchased from commercial suppliers at highest possible purity.

Electrospray ionization mass spectrometry (ESI-MS) was performed on a Bruker compact ESI-Q-TOF mass spectrometer with positive mode. A THF solution of cluster samples was prepared by dissolving the powder sample in degassed THF just before the direct infusion (3 μL/min).

4.2 NHC salts

Synthesis of NHC salts were adapted from a published procedure.[4] In a 15 mL pressure tube, 5 mL of acetonitrile was added to benzimidazole (0.590 g, 5.00 mmol). Powdered potassium carbonate (1.04 g, 7.50 mmol), was added to the mixture with 2 mL of acetonitrile. The reaction mixture was sealed and heated to 80 °C for 30 min. In the synthesis of **1a**, benzyl bromide (1.25 mL, 10.5 mmol) was then added dropwise, and the pressure tube was sealed and stirred at 85 °C for further 72 h. Other NHC salts were synthesized with 10.5 mmol of the desired wingtip group. The reaction mixture was removed from heat and concentrated using compressed air flow. Following this, 7 mL of water and 7 mL of dichloromethane were added to the pressure tube, and the solid product was collected by filtration, washed with diethyl ether (10 mL x 3 times) and dried in vacuo (1.68 g, 88.8 %).

4.3 Gold Complexes

Synthesis of the NHC-Au-X gold complexes were adapted from a published procedure.[3] The NHC salt (0.134 g, 0.353 mmol), gold(I) dimethylsulfide (0.104 g, 0.353 mmol), and potassium carbonate (0.500 g, 3.6 mmol) were suspended in 100 mL of acetone in a 250 mL round-bottomed flask. This reaction mixture was stirred at room temperature for 1 h and then refluxed at 65 °C for 16 h. The hot reaction mixture was filtered through a coarse frit and dried in vacuo. The beige product was then dissolved in min. dichloromethane and filtered through a 1 cm silica plug. The filtrate was dried in vacuo, and the white product was collected. Excess DCM was removed by washing with 10 mL pentane and drying the sample thoroughly (0.147 g, 72.3 %).

4.4 $[Au_{11}(NHC)_8Br_2]Br$

WARNING: Potassium graphite (KC_8) is a pyrophoric solid and should be handled under inert atmosphere. Unreacted KC_8 and any vessel which came in contact with KC_8 were quenched using a solution of butylated hydroxytoluene (BHT) in THF under inert atmosphere.

In a N_2 filled glovebox, **2a** (0.059 g, 0.1 mmol) and dibenzo-18-crown-6 (0.024 g, 0.066 mmol) were dissolved in 18.5 mL of dry THF and cooled to -40 °C in the glovebox freezer. The solution was added to KC_8 (0.028 g, 0.20 mmol) in a 100 mL Schlenk flask and stirred in an ice bath. The reaction was monitored by examining aliquots of the reaction mixture every 30 minutes, removed by syringe, by UV-Vis. After confirmation of the completed reaction, when the observed 420 nm peak was 10 % of the 290 nm peak, the THF was removed by exposure of the reaction mixture to vacuum in a Schlenk line. Upon dryness, the flask was taken back into the glovebox, where the crude of the reaction was dissolved in 20 mL of THF and filtered through Celite® into a 100 mL round bottom flask (RBF). To the RBF, 40 mL of pentane were added to precipitate out **3**. The precipitate was collected in a Celite® plug, and the solid was washed with 10 mL of ether. The collected solid was subsequently washed through with 7 mL of THF, and the resulting extracts precipitated with 14 mL of pentane. The supernatant was removed, and precipitation was repeated twice more until the starting material and dibenzo-18-crown-6 were no longer seen in the UV-Vis spectrum as evidenced by the removal of a shoulder peak at 282 nm. This procedure results in a red powder which is primarily $[Au_{11}(NHC)_8Br_2]Br$ (0.027 g, 62 % yield, 81 % purity by ^1H NMR integration).

To achieve **3** of higher purity, the red powder was dissolved in 9 mL of THF, and 1 mL of pentane was added to this solution.

The solution was then filtered through Celite® and the filtrate removed *in vacuo*. This process was repeated two times or until impurities were under 85.1 % based on ^{1}H NMR determinations. Pure crystals can be obtained in low yield by layering cold heptane (-40 °C) over a dilute solution of **2a** in THF (4:5 heptane:THF). The crystals were washed with 2 x 5 mL of cold THF (-40 °C), dried in vacuo and dissolved in CD_2Cl_2. Pure ^{1}H NMR and $^{13}C\{^{1}H\}$ NMR were obtained using these crystals.

ASSOCIATED CONTENT

Supporting Information. Characterization data including NMR characterization of all materials, UV-Vis spectra and ESI-MS of **3**. This material is available free of charge via the Internet at http://pubs.acs.org.

AUTHOR INFORMATION

Corresponding Author

* **Cathleen M. Crudden** – *Department of Chemistry, Queen's University, Kingston, Ontario K7L 3N6, Canada; Institute of Transformative BioMolecules (WPI-ITbM), Nagoya University Furo, Chikusa, Nagoya 464-8602, Japan; orcid.org/0000-0003-2154-8107;* Email: cruddenc@chem.queensu.ca

* **Tatsuya Tsukuda** – *Department of Chemistry, Graduate School of Science, The University of Tokyo, Bunkyo-ku, Tokyo 113-0033, Japan;* orcid.org/0000-0002-0190- 6379; Email: tsukuda@chem.s.u-tokyo.ac.jp
tsukuda@chem.s.u-tokyo.ac.jp

* Hannu Häkkinen – *Departments of Chemistry and Physics, Nanoscience Center, University of Jyväskylä, 40014 Jyväskylä, Finland*; orcid.org/0000-0002-8558-5436; Email: hannu.j.Hakkinen@jyu.fi

Present Addresses

† Institute of Transformative Bio-Molecules (WPI-ITbM), Nagoya University, Chikusa, Nagoya 464-8602, Japan

ACKNOWLEDGMENTS

CMC thanks the Natural Sciences and Engineering Research Council (NSERC) and the Social Sciences and Humanities Research Council (SSHRC) for funding this work through the NSERC discovery and New Frontiers in Research Funds. CMC also thanks the Canada Foundation for Innovation (CFI) and the Ontario Research Fund (ORF) for support of this work.

TT would like to thank JSPS KAKENHI (20H00370) and JST CREST (JPMJCR20B2) for financial support.

HH acknowledges the support from the Academy of Finland (grant 315549).

AIS would like to acknowledge NSERC for a CGS-M, the Ontario government for an OGS, and Queen's University for the Robins excellence award scholarship. AIS would like to thank Dr. Hong Yi for performing ESI-MS experiments which are not included in the manuscript, but aided in understanding. AIS would like to thank Dr. Gabriele Schatte for help with XRD determinations and Dr. Francoise Sauriel for helpful discussions about NMR interpretation.

REFERENCES

(1) Chakraborty, I.; Pradeep, T. Atomically Precise Clusters of Noble Metals: Emerging Link between Atoms and Nanoparticles. *Chem. Rev.* **2017,** *117*, 8208-8271.

(2) Mingos, D. M. P. Historical Introduction to Gold Colloids, Clusters and Nanoparticles. In *Gold Clusters, Colloids, and Nanoparticles I;* Structure and Bonding, Vol. 161; Springer, Cham, 2014; pp. 1-47.

(3) Narouz, M. R.; Takano, S.; Lummis, P. A.; Levchenko, T. I.; Nazemi, A.; Kaappa, S.; Malola, S.; Yousefalizadeh, G.; Calhoun, L. A.; Stamplecoskie, K. G.; Hakkinen, H.; Tsukuda, T.; Crudden, C. M. Robust, Highly Luminescent Au_{13} Superatoms Protected by N-Heterocyclic Carbenes. *J. Am. Chem. Soc.* **2019,** *141*, 14997-15002.

(4) Narouz, M. R.; Osten, K. M.; Unsworth, P. J.; Man, R. W. Y.; Salorinne, K.; Takano, S.; Tomihara, R.; Kaappa, S.; Malola, S.; Dinh, C.-T.; Padmos, J. D.; Ayoo, K.; Garrett, P. J.; Nambo, M.; Horton, J. H.; Sargent, E. H.; Häkkinen, H.; Tsukuda, T.; Crudden, C. M. N-Heterocyclic Carbene-Functionalized Magic-Number Gold Nanoclusters. *Nat. Chem.* **2019,** *11*, 419-425.

(5) Robilotto, T. J.; Bacsa, J.; Gray, T. G.; Sadighi, J. P. Synthesis of a Trigold Monocation: An Isolobal Analogue of $[H_3]^+$. *Angew. Chem. Int. Ed.* **2012,** *51*, 12077-12080.

(6) Jin, L. Q.; Weinberger, D. S.; Melaimi, M.; Moore, C. E.; Rheingold, A. L.; Bertrand, G. Trinuclear Gold Clusters Supported by Cyclic (alkyl)(amino)carbene Ligands: Mimics for Gold Heterogeneous Catalysts. *Angew. Chem. Int. Ed.* **2014,** *53*, 9059-9063.

(7) Man, R. W. Y.; Yi, H.; Malola, S.; Takano, S.; Tsukuda, T.; Häkkinen, H.; Nambo, M.; Crudden, C. M. Synthesis and Characterization of Enantiopure Chiral Bis NHC-Stabilized Edge-Shared Au_{10} Nanocluster with Unique Prolate Shape. *J. Am. Chem. Soc.* **2022,** *144*, 2056-2061.

(8) Luo, P.; Bai, S.; Wang, X.; Zhao, J.; Yan, Z. N.; Han, Y. F.; Zang, S. Q.; Mak, T. C. W. Tuning the Magic Sizes and Optical Properties of Atomically Precise Bidentate N-Heterocyclic Carbene-Protected Gold Nanoclusters via Subtle Change of N-Substituents. *Adv. Opt. Mater.* **2021,** *9*, 2001936.

(9) Shen, H.; Xiang, S. J.; Xu, Z.; Liu, C.; Li, X. H.; Sun, C. F.; Lin, S. C.; Teo, B. K.; Zheng, N. F. Superatomic Au_{13} Clusters Ligated by Different N-heterocyclic Carbenes and their Ligand-Dependent Catalysis, photoluminescence, and Proton Sensitivity. *Nano. Res.* **2020,** *13*, 1908-1911.

(10) Yi, H.; Osten, K. M.; Levchenko, T. I.; Veinot, A. J.; Aramaki, Y.; Ooi, T.; Nambo, M.; Crudden, C. M. Synthesis and Enantioseparation of Chiral Au_{13} Nanoclusters Protected by bis-N-Heterocyclic Carbene Ligands. *Chem. Sci.* **2021**, 12, 10436-10440.

(11) Hirano, K.; Takano, S.; Tsukuda, T. Ligand Effects on the Structures of $[Au_{23}L_6(C{\equiv}CPh)_9]^{2+}$ (L = N-Heterocyclic Carbene vs Phosphine) with Au_{17} Superatomic Cores. *J. Phys. Chem. C.* **2021,** *125*, 9930-9936.

(12) Kulkarni, V. K.; Khiarak, B. N.; Takano, S.; Malola, S.; Albright, E. L.; Levchenko, T. I.; Aloisio, M. D.; Dinh, C.-T.; Tsukuda, T.; Häkkinen, H.; Crudden, C. M. N-Heterocyclic Carbene-Stabilized Hydrido Au_{24} Nanoclusters: Synthesis, Structure, and Electrocatalytic Reduction of CO_2. *J. Am. Chem. Soc.* **2022,** *144*, 9000-9006.

(13) Shen, H.; Tang, X.; Wu, Q.; Zhang, Y.; Ma, C.; Xu, Z.; Teo, B. K.; Zheng, N. Guiding the High-Yield Synthesis of NHC-Ligated Gold Nanoclusters by ^{19}F NMR Spectroscopy. *ACS Nanosci. Au* **2022,** *2*, 520-526.

(14) Shen, H.; Deng, G. C.; Kaappa, S.; Tan, T. D.; Han, Y. Z.; Malola, S.; Lin, S. C.; Teo, B. K.; Hakkinen, H.; Zheng, N. F. Highly Robust but Surface-Active: An N-Heterocyclic Carbene-Stabilized Au_{25} Nanocluster. *Angew. Chem. Int. Ed.* **2019,** *58*, 17731-17735.

(15) Lummis, P. A.; Osten, K. M.; Levchenko, T. I.; Sabooni Asre Hazer, M.; Malola, S.; Owens-Baird, B.; Veinot, A. J.; Albright, E. L.; Schatte, G.; Takano, S.; Kovnir, K.; Stamplecoskie, K. G.; Tsukuda, T.; Häkkinen, H.; Nambo, M.; Crudden, C. M. NHC-Stabilized Au_{10} Nanoclusters and Their Conversion to Au_{25} Nanoclusters. *J. Am. Chem. Soc. Au* **2022,** *2*, 875-885.
(16) Shen, H.; Xu, Z.; Hazer, M. S. A.; Wu, Q.; Peng, J.; Qin, R.; Malola, S.; Teo, B. K.; Hakkkinen, H.; Zheng, N. F. Surface Coordination of Multiple Ligands Endows N-Heterocyclic Carbene-Stabilized Gold Nanoclusters with High Robustness and Surface Reactivity. *Angew. Chem. Int. Ed.* **2021,** 60, 3752-3758.
(17) Goswami, N.; Yao, Q. F.; Chen, T. K.; Xie, J. P. Mechanistic Exploration and Controlled Synthesis of Precise Thiolate-gold Nanoclusters. *Coord. Chem. Rev.* **2016,** *329*, 1-15.
(18) Zhu, M. Z.; Qian, H. F.; Jin, R. C. Thiolate-Protected $Au_{24}(SC_2H_4Ph)_{20}$ Nanoclusters: Superatoms or Not? *J. Phys. Chem. Lett.* **2010,** *1*, 1003-1007.
(19) Zhu, M.; Lanni, E.; Garg, N.; Bier, M. E.; Jin, R. Kinetically Controlled, High-Yield Synthesis of Au_{25} Clusters. *J. Am. Chem. Soc.* **2008,** *130*, 1138-1139.
(20) Zhu, M. Z.; Qian, H. F.; Jin, R. C. Thiolate-Protected Au_{20} Clusters with a Large Energy Gap of 2.1 eV. *J. Am. Chem. Soc.* **2009,** *131*, 7220-7221.
(21) Yu, Y.; Chen, X.; Yao, Q. F.; Yu, Y.; Yan, N.; Xie, J. P. Scalable and Precise Synthesis of Thiolated Au_{10-12}, Au_{15}, Au_{18}, and Au_{25} Nanoclusters via pH Controlled CO Reduction. *Chem. Mater.* **2013,** *25*, 946-952.
(22) Yu, Y.; Luo, Z. T.; Yu, Y.; Lee, J. Y.; Xie, J. P. Observation of Cluster Size Growth in CO-Directed Synthesis of $Au_{25}(SR)_{18}$ Nanoclusters. *ACS Nano.* **2012,** *6*, 7920-7927.
(23) Wu, Z. K.; MacDonald, M. A.; Chen, J.; Zhang, P.; Jin, R. C. Kinetic Control and Thermodynamic Selection in the Synthesis of Atomically Precise Gold Nanoclusters. *J. Am. Chem. Soc.* **2011,** *133*, 9670-9673.
(24) Yao, Q.; Yu, Y.; Yuan, X.; Yu, Y.; Xie, J.; Lee, J. Y. Two-Phase Synthesis of Small Thiolate-Protected Au_{15} and Au_{18} Nanoclusters. *Small* **2013,** *9*, 2696-2701.
(25) Ghosh, A.; Udayabhaskararao, T.; Pradeep, T. One-Step Route to Luminescent $Au_{18}SG_{14}$ in the Condensed Phase and Its Closed Shell Molecular Ions in the Gas Phase. *J. Phys. Chem. Lett.* **2012,** *3*, 1997-2002.
(26) Bartenbach, D.; Wenzel, O.; Popescu, R.; Faden, L.-P.; Reiß, A.; Kaiser, M.; Zimina, A.; Grunwaldt, J.-D.; Gerthsen, D.; Feldmann, C. Liquid-Phase Synthesis of Highly Reactive Rare-Earth Metal Nanoparticles. *Angew. Chem. Int. Ed.* **2021,** *60*, 17373-17377.
(27) Briant, C. E.; Theobald, B. R. C.; White, J. W.; Bell, L. K.; Mingos, D. M. P.; Welch, A. J. Synthesis and X-Ray Structural Characterization of the Centered Icosahedral Gold Cluster Compound $[Au_{13}(PMe_2Ph)_{10}Cl_2](PF_6)_3$ - the Realization of a Theoretical Prediction. *J. Chem. Soc. Chem. Comm.* **1981,** 5, 201-202.
(28) Copley, R. C. B.; Mingos, M. P. The Novel Structure of the $[Au_{11}(PMePh_2)_{10}]^{3+}$ Cation: Crystal Structures of $[Au_{11}(PMePh_2)_{10}][C_2B_9H_{12}]_3\bullet 4$thf and $[Au_{11}(PMePh_2)_{10}][C_2B_9H_{12}]_3$ (thf = tetrahydrofuran). *J. Chem. Soc. Dalton.* **1996,** 4, 479-489.
(29) Mingos, D. M. P.; Hall, K. P. Homo- and Heteronuclear Cluster Compounds of Gold. *Prog. Inorg. Chem.* **1984,** *64*, 237-325.
(30) Fetzer, F.; Schrenk, C.; Pollard, N.; Adeagbo, A.; Clayborne, A. Z.; Schnepf, A. A New Reductant in Gold Cluster Chemistry Gives a Superatomic Gold Gallium Cluster. *Chem. Commun.* **2021,** *57*, 3551-3554.
(31) Ramsay, H. S.; Silverman, M. M.; Simon, D.; Oleschuk, R. D.; Stamplecoskie, K. G. Light Activated Synthesis of the Atomically Precise Fluorescent Silver Cluster $Ag_{18}(Capt)_{14}$. *Nanoscale* **2019,** *11*, 20522-20526.
(32) Schöttle, C.; Bockstaller, P.; Popescu, R.; Gerthsen, D.; Feldmann, C. Sodium-Naphthalenide-Driven Synthesis of Base-Metal Nanoparticles and Follow-up Reactions. *Angew. Chem. Int. Ed.* **2015,** *54*, 9866-9870.
(33) Schöttle, C.; Bockstaller, P.; Gerthsen, D.; Feldmann, C. Tungsten Nanoparticles from Liquid-Ammonia-Based Synthesis. *Chem. Commun.* **2014,** *50*, 4547-4550.
(34) Shichibu, Y.; Negishi, Y.; Watanabe, T.; Chaki, N. K.; Kawaguchi, H.; Tsukuda, T., Biicosahedral Gold Clusters $[Au_{25}(PPh_3)_{10}(SC_nH_{2n+1})_5Cl_2]^{2+}$ (n = 2−18): A Stepping Stone to Cluster-Assembled Materials. *J. Phys. Chem. C* **2007,** *111*, 7845-7847.
(35) McKenzie, L. C.; Zaikova, T. O.; Hutchison, J. E. Structurally Similar Triphenylphosphine-Stabilized Undecagolds, $Au_{11}(PPh_3)_7Cl_3$ and $[Au_{11}(PPh_3)_8Cl_2]Cl$, Exhibit Distinct Ligand Exchange Pathways with Glutathione. *J. Am. Chem. Soc.* **2014,** *136*, 13426-13435.
(36) Collado, A.; Gomez-Suarez, A.; Martin, A. R.; Slawin, A. M. Z.; Nolan, S. P., Straightforward Synthesis of [Au(NHC)X] (NHC = N-heterocyclic carbene, X = Cl, Br, I) Complexes. *Chem. Commun.* **2013,** *49*, 5541-5543.
(37) Smits, J. M. M.; Beurskens, P. T.; Steggerda, J. J. Gold Phosphine Cluster Compounds: Chemical and Crystallographic Difficulties. *J. Crystallogr. Spectrosc. Res.* **1983,** *13*, 381-384.
(38) Gutrath, B. S.; Englert, U.; Wang, Y.; Simon, U. A Missing Link in Undecagold Cluster Chemistry: Single-Crystal X-ray Analysis of $[Au_{11}(PPh_3)_7Cl_3]$. *Eur. J. Inorg. Chem.* **2013,** *2013*, 2002-2006.
(39) An 84 % pure sample of **3** was employed in these experiments. Since the overall stability of the clusters is close to phosphine analogs prepared by Hutchison, we do not believe that the presence of impurities had a large effect on the stability studies.
(40) Enkovaara, J.; Rostgaard, C.; Mortensen, J. J.; Chen, J.; Dułak, M.; Ferrighi, L.; Gavnholt, J.; Glinsvad, C.; Haikola, V.; Hansen, H. A.; Kristoffersen, H. H.; Kuisma, M.; Larsen, A. H.; Lehtovaara, L.; Ljungberg, M.; Lopez-Acevedo, O.; Moses, P. G.; Ojanen, J.; Olsen, T.; Petzold, V.; Romero, N. A.; Stausholm-Møller, J.; Strange, M.; Tritsaris, G. A.; Vanin, M.; Walter, M.; Hammer, B.; Häkkinen, H.; Madsen, G. K. H.; Nieminen, R. M.; Nørskov, J. K.; Puska, M.; Rantala, T. T.; Schiøtz, J.; Thygesen, K. S.; Jacobsen, K. W. Electronic Structure Calculations with GPAW: a Real-Space Implementation of the Projector Augmented-Wave Method. *J. Phys. Condens. Matter* **2010,** *22*, 253202.
(41) Perdew, J. P.; Burke, K.; Ernzerhof, M. Generalized Gradient Approximation Made Simple. *Phys. Rev. Lett.* **1996,** *77*, 3865-3868.
(42) Wellendorff, J.; Lundgaard, K. T.; Møgelhøj, A.; Petzold, V.; Landis, D. D.; Nørskov, J. K.; Bligaard, T.; Jacobsen, K. W. Density Functionals for Surface Science: Exchange-Correlation Model Development with Bayesian Error Estimation. *Phys. Rev. B* **2012,** *85*, 235149.
(42) Walter, M.; Akola, J.; Lopez-Acevedo, O.; Jadzinsky, P. D.; Calero, G.; Ackerson, C. J.; Whetten, R. L.; Grönbeck, H.; Häkkinen, H. A Unified View of Ligand-Protected Gold Clusters

as Superatom Complexes. *Proc. Natl. Acad. Sci. U S A* **2008,** *105,* 9157-9162.

Table of Contents Graphic